Simulations of alternative phases of space-filling graphene crystals under mechanical loads

Peter W. Chung*

US Army Research Laboratory, AMSRL-CI-HC, Aberdeen Proving Ground MD 21005, USA

Abstract

Quantum-level density functional simulations of planar graphene subjected to mechanical strains are found to develop monoclinic or nearly-orthorhombic crystal structures through second-order phase transitions. They are achieved through a bond rotation similar in part to the Stone–Wales transformation. The key result is the observation of the rotation in even the smallest primitive cell, which connects to the transformation through the space-filling crystal concept. Contrary to earlier observations of phase change in graphene, the deformations needed to obtain the configurations exhibit both kinetic and thermodynamic features.

Keywords: Solid–solid phase change; graphene crystals; Stone–Wales transformation; Materials simulation

1. Introduction

Since their discovery [1,2], intense interest has focused on the engineering of materials and devices from various forms of elemental carbon. The readily encountered single-crystal form of single-wall carbon nanotubes continues to be explored for its many possible uses [3,4] and subsequent engineering applications [5,6]. In many of the latter developments, it is important to understand the mechanical behavior of elemental carbon forms and, in general, its mechanics, outside of the standard linear elastic regime. Significant progresses have been made in recent years in this regard by examining the mechanical limits of nanotubes and graphene. Of particular interest has been the identification and simulation of the so-called Stone–Wales (SW) transformation [7], a mechanism that has a critical role in the mechanical deformation of nanotubes and fullerenes under tension near the yield point [8–19].

The SW mechanism is basically a rotation of a bond connecting two atoms that changes the local coordination, equivalent to a local phase transformation of the material. The rotation is accompanied by a local relaxation of the lattice in the neighborhood of the bond, leaving a new configuration that is energetically more favorable and that relieves the amount of strain energy that the system must withstand [10]. Its particularly interesting feature is that it is a mechanically induced effect with multiaxial features, unlike the hydrostatic-pressure-or temperature-induced behavior historically known for carbon forms [20,21]. The importance of SW to understanding plasticity [11], nanotube yield [10–12, 14, 22, 23], geometry dependence [9], and dependence on realistic experimental conditions [24,25] have been well documented.

In a typical kinetic simulation of strains in a large lattice, the SW defect forms spontaneously at random locations, with some preferable orientation according to the zig-zag (ZZ) or armchair (AC) configurations of the basal plane [10–12]. Generally, the theoretical investigations thus far have considered relatively large supercells of atoms in graphene and nanotubes or formation studies of molecular fullerenes. This presumes that the defect will form at some location. In contrast to this, we assume that the motion occurs *everywhere*. The point of departure, therefore, is in the selection of a periodic primitive cell to perform our calculations using mechanical uniaxial loading conditions. This effectively isolates the bond-rotation effect from other parametric dependencies, so that we can examine the mechanics separately and decouple the longitudinal and transverse directions to study the anisotropy of the material.

In this paper, we offer an alternative mechanical interpretation of previously observed results, i.e. that the defect formation is related, in part, to a zero-

* Tel.: +1 410 278 6027; Fax: +1 410 278 4983; E-mail: pchung@arl.army.mil

Computational Fluid and Solid Mechanics 2005
K.J. Bathe (Editor)

temperature-limiting behavior of a deformation-induced solid–solid phase transformation. We compute the entire strain energy landscape for a periodic primitive cell undergoing large deformations and examine differences in the results as they depend on the orientation of the basal plane. To contrast this with earlier works, the key result here is that the rotation event not only occurs but is observable even in the smallest primitive cell, interacting with its images, which subsequently suggests a second-order phase change in the sense of a space-filling crystal [26]. Though previously shown to be a kinetic process, we further show through constrained uniaxial deformations that bond rotations possess both kinetic and thermodynamic features depending on the axis of loading.

2. Calculation procedure

We use the concepts of finite strain continuum mechanics for the definitions of deformations and strains. Points in the reference configuration are defined by $\mathbf{X}$ and their corresponding points in the deformed configuration by $\mathbf{x}$. The deformation gradient tensor is then defined as the gradient of $\mathbf{x}$ with respect to the reference configuration $\mathbf{X}$, such that $\mathbf{F} = \nabla_o \mathbf{x} = \partial \mathbf{x}/\partial \mathbf{X}$. Consideration is presently limited to uniaxial stretching along either the principal ZZ or AC axes of the graphene sheet, with the former aligned along the basal plane and the latter oriented transversely. This simplifies the deformation tensor to a diagonal 3×3 matrix whose components are $(1 + \alpha, 1 + \beta, 1)$, where, for all parametric variations of α, β is currently held fixed at zero and, likewise, for all β variations, α is set to zero. In a one-dimensional sense, α and β are the so-called engineering strains that measure the uniaxial change in length relative to the reference length. Discussions henceforth interchangeably use the term 'deformation' to refer to the relevant component of $\mathbf{F}$ being used and the term '*strain*' to refer to the respective engineering strain component, i.e. in the context of this paper, deformation is 1 + (strain). Deformations are then applied in the conventional way by multiplying $\mathbf{A}_i$ for $i = 1, 2, 3$ by $\mathbf{F}$ to give the deformed lattice vectors $\mathbf{a}_i = \Sigma_{j=1,2,3} (\mathbf{F})_{ij} \mathbf{A}_j$.

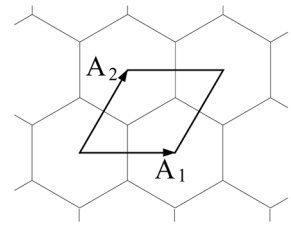

Fig. 1. Graphene primitive cell.

The calculations proceed by taking the periodic cell of single-crystal graphene containing two atoms in the primitive basis, as shown in Fig. 1. One atom is held fixed while the position of the other atom is varied in the plane. At each deformation state where we hold $\mathbf{a}_i$ fixed, 2200 grid points are evaluated using density functional theory (DFT) [27] from the planewave ABINIT code [28], in which the exchange and correlation term is treated through the generalized gradient approximation (GGA) according to the Perdew–Burke–Ernzerhof functional [29] with the Hartwigsen–Goedecker–Hutter pseudopotential for carbon. A planewave energy cutoff of 1360 eV is used throughout. Each grid point represents a single self-consistent fluid (SCF) calculation and the points combine to generate a full energy landscape.

3. Results and discussion

Calculations of strain energies are shown in Fig. 2 in the unloaded reference state and at 29% strain in both the ZZ and the AC directions. To be able to compare the results as they change with deformation, we normalize the cell dimensions so that (0,0) signifies the origin of the local coordinate frame in the lower left corner of the cell, (1,0) signifies the lower right corner, etc. In the undeformed case with the fixed position of the first atom at the reduced coordinate of (1/3,1/3), the equilibrium position of the second atom is clearly at (2/3,2/3). The

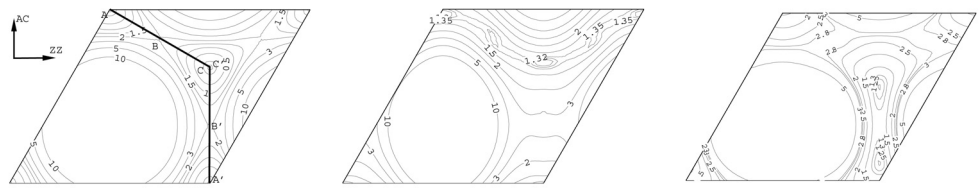

(a) Zero strain (b) 29% ZZ strain (c) 29% AC strain

Fig. 2. Strain energy landscapes. Primitive cell dimensions are normalized.

additional minima at (1,0), (1,1), and (0,1) represent the crystal symmetries.

At 29% strain, there is a clear change from hexagonal structure – two additional local minima appear in the cell. Figure 2b shows these to be at (1/3,5/6) and (5/6, 5/6) at an energy of 1.32 eV per primitive cell atom. The reverse barrier is approximately 50 meV per atom at this strain, suggesting a total activation of 1.37 eV per atom. The barrier height is very high due to the assumption of a space-filling crystal that does not allow for relaxation in the vicinity of the defect. The SW formation depends critically on the local strain fields in the region [14], and the disabling of this relaxation makes a direct quantitative comparison difficult. However, the values can still be reasonably compared by considering that the energy of all atoms participating in the rotation is 2.74 eV. It is noteworthy the minima actually appear for such a small system, expedited by the applied mechanical loads, and the character is kinetic, as evident by a nonzero reverse barrier.

This activation corresponds to a transformation stress of 24.9 GPa, assuming a graphene layer thickness of 3.35 Å. The transformation occurs at approximately 29% engineering strain. These values are in reasonable agreement with earlier calculations that show nanotube yield strains of 5–30% [22] and SW defect activation energies of 3–8 eV via theory [8,9,30] and 4–10 eV via experiments [13,31–33]. Experimental tensile strengths are in the range 10–150 GPa [23,34].

The behavior for uniaxial tension along the AC axis is considerably different. The second minimum that appears in Fig. 2c is from the minimum originally at (1,0) that travels upward with increasing deformation. The result is a reduction in the symmetry of the crystal without the creation of new minima. The midpoint along the line connecting the minima corresponds to the exact orthorhombic structure. These observations appear to be consistent with findings that the defect appearance depends on chirality [10–12]. However, it is noteworthy that it is a gradual closening of the minima, rather than a spontaneous activation, suggesting a thermodynamic behavior.

The kinetic and thermodynamic properties of the deformations are made more evident in Fig. 3 in the energy levels along the lines ABC and A′B′C′ from Fig. 2a. At the 29% ZZ strain, a new minimum appears and takes over at B with increasing strain. Up to 29% and high AC strains, the minima that originally were at A′ and C′ grow closer to B′, but a new minimum does not take over.

These results appear to suggest two alternative crystal configurations under our presumptions of uniaxial mechanical loading at zero temperature and the space-filling crystal concept. In the ZZ direction the crystal takes a monoclinic form, and in the AC direction the

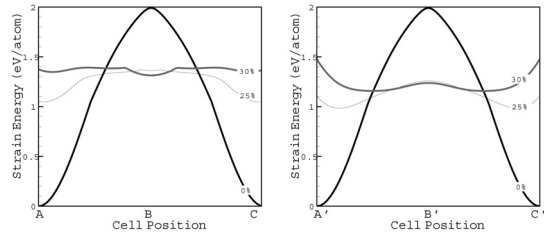

(a) ZZ (b) AC

Fig. 3. Energy with respect to deformation along lines ABC and A′B′C′ of Fig. 2a.

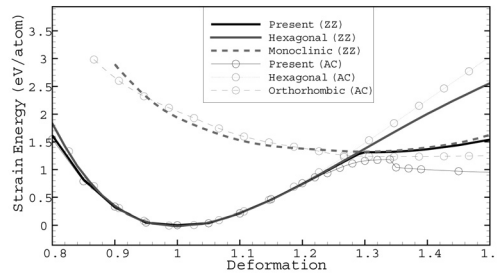

Fig. 4. Alternative crystal strain energies.

form is nearly orthorhombic. The latter is made conditional because of the thermodynamic feature of the bond rotation described earlier. The strain energies of the hypothetically deforming crystals in Fig. 4 demonstrate that the lowest-energy paths follow these alternative structures. In the case of AC straining, however, the crystal finds a lower energy configuration a small distance from the exact orthorhombic structure. Also noteworthy is the smaller curvature of the two alternative crystal forms, which signifies a softer material behavior and helps to explain the exclusivity of the defect formation in a small neighborhood around the rotating bond.

4. Conclusions

The current results have an implied assumption of zero temperatures through static density functional theory (DFT) calculations. Indeed, experimental evidence suggests that the bond rotation is a localized event where temperature effects are critical. One also expects that in the configuration space of the material where both temperature and deformations are accounted for, the regime where these phase transformations are valid is asymptotically smaller than for general SW transformations. However, our approach for decoupling the

temperature from the mechanics and using the simpler space crystal assumption reveal new facets to the SW phenomenon. The observations that the defect formation may be interpreted as a partial concerted phase transformation and that the behavior exhibits thermodynamic anisotropy do not appear to have been considered before and shed new understanding on this important material effect.

Acknowledgments

The author gratefully acknowledges discussions with Richard D. James and Deepak Srivastava and the support from the US Army Research Laboratory Director's Research Initiative Award (DRIFY04). Significant computer resources were made available through the US Army Research Laboratory Major Shared Resource Center.

References

[1] Kroto HW, Heath JR, O'Brien SC, Curl RF, Smalley RE. C-60 buckminsterfullerene. Nature 1985;318:162.
[2] Iijima S. Helical microtubules of graphitic carbon. Nature 1991;354:56.
[3] Tans SJ, Devoret MH, Dai H, Thess A, Smalley RE, Geerligs LJ, Dekker C. Individual single-wall carbon nanotubes as quantum wires. Nature 1997;386:474.
[4] Liu C, Fan YY, Cong HT, Cheng HM, Dresselhaus MS. Hydrogen storate in single-walled carbon nanotubes at room temperature. Science 1999;286:1127–1129.
[5] Kumar S, Dang TD, Arnold FE, Bhattacharyya AR, Min BG, Zhang X, Vaia RA, Park C, Adams WW, Hauge R, Smalley RE, Ramesh S, Willis PW. Synthesis, structure and properties of pbo/swnt composites. Macromolecules 2002;35:9039.
[6] Wagner HD, Lourie O, Feldman Y, Tenne R. Stress-induced fragmentation of multiwall carbon nanotubes in a polymer matrix. Appl Phys Lett 1998;72:188.
[7] Stone AJ, Wales DJ. Theoretical studies of icosahedral c60 and some related species. Chem Phys Lett 1986;128:501–503.
[8] Samsonidze GG, Samsonidze GG, Yakobson BI. Kinetic theory of symmetry-dependent strength in carbon nanotubes. Phys Rev Lett 2002;88:1–4.
[9] Zhou LG, Shi S-Q. Formation energy of stone-wales defects in carbon nanotubes. Appl Phys Lett 2003;83:1222–1224.
[10] Nardelli MB, Yakobson BI, Bernholc J. Mechanism of strain release in carbon nanotubes. Phys Rev B 1998;57:4277–4280.
[11] Yakobson BI. Mechanical relaxation and 'intramolecular plasticity' in carbon nanotubes. Appl Phys Lett 1998;72:918–920.
[12] Zhang P, Lammert PE, Crespi VH. Plastic deformations of carbon nanotubes. Phys Rev Lett 1998;81:5346–5349.
[13] Kaxiras E, Pandey KC. Energetics of defects and diffusion mechanisms in graphite. Phys Rev Lett 1988;61:2693–2696.
[14] Yakobson BI, Samsonidze GG, Samsonidze GG. Atomistic theory of mechanical relaxation in fullerene nanotubes. Carbon 2000;38:1675–1680.
[15] Samsonidze GG, Samsonidze GG, Yakobson BI. Energetics of Stone–Wales defects in deformations of monoatomic hexagonal layers. Comput Mater Sci 2002;23:62–72.
[16] Troya D, Mielke SL, Schatz GC. Carbon nanotube fracture – difference between quantum mechanical mechanisms and those of empirical potentials. Chem Phys Lett 2003;382:133–141.
[17] Belytschko T, Xiao SP, Schatz GC, Ruoff RS. Atomistic simulations of nanotube fracture. Phys Rev B 2002;65:235430–1–8.
[18] Dresselhaus MS, Dresselhaus G, Eklund PC. Science of Fullerenes and Carbon Nanotubes. San Diego; Academic Press, 1996.
[19] Bettinger HF, Yakobson BI, Scuseria GE. Scratching the surface of the buckminsterfullerene: the barriers for Stone–Wales transformation through symmetric and asymmetric transition states. J Am Chem Soc 2003;125:5572–5580.
[20] Ergun S. Structure of carbon. Carbon 1968;6:141–159.
[21] Bundy FP, Bassett WA, Weathers MS, Hemley RJ, Mao HK, Goncharov AF. The pressure–temperature phase and transformation diagram for carbon: updated through 1994. Carbon 1996;34:141–153.
[22] Yakobson BI, Campbell MP, Brabec CJ, Bernholc J. High strain rate fracture and c-chain unraveling in carbon nanotubes. Comput Mater Sci 1997;8:341–348.
[23] Yu M-F, Lourie O, Dyer MJ, Moloni K, Kelly TF, Ruoff RS. Strength and breaking mechanism of multiwalled carbon nanotubes under tensile load. Science 2000;287:637–640.
[24] Wei C, Cho K, Srivastava D. Tensile strength of carbon nanotubes under realistic temperature and strain rate. Phys Rev B 2003;67:115407–1–6.
[25] Dumitrica T, Yakobson BI. Strain-rate and temperature dependent plastic yield in carbon nanotubes from ab initio calculations. Appl Phys Lett 2004;84:2775–2777.
[26] Lifshitz EM, Pitaevskii LP. Physical Kinetics. Oxford: Butterworth Heinemann, 1981.
[27] Hohenberg P, Kohn W. Inhomogeneous electron gas. Phys Rev 1964;136:B864–B871.
[28] Gonze X, Beuken J-M, Caracas R, Detraux F, Fuchs M, Rignanese G-M, Sindic L, Verstraete M, Zerah G, Jollet F, Torrent M, Roy A, Mikami M, Ghosez P, Raty J-Y, Allan DC. First-principles computation of material properties: the abinit software project. Comput Mater Sci 2002;25:478–492.
[29] Perdew JP, Burke K, and Ernzerhof M. Generalized gradient approximation made simple. Phys Rev Lett 1996;77:3865–3868.
[30] Crespi VH, Benedict LX, Cohen ML, Louie SG. Prediction of a pure-carbon planar covalent metal. Phys Rev B 1996;53:13303–13305.

[31] Kanter MA. Diffusion of carbon atoms in natural graphite crystals. Phys Rev 1957;107:655–663.
[32] Dienes GJ. Mechanism for self-diffusion in graphite. J Appl Phys 1952;23:1194–1200.
[33] Xu CH, Fu CL, Pedraza DF. Simulations of point-defect properties in graphite by a tight-binding-force model. Phys Rev B 1993;48:13273–13279.
[34] Demczyk BG, Yang YM, Cumings J, Hetman M, Han W, Zettl A, Ritchie RO. Direct mechanical measurement of the tensile strength and elastic modulus of multiwalled carbon nanotubes. Mater Sci Eng A 2002;334:173–178.